Article:
Abbasi, E. and Rainforth, W.M. (2017) Microstructural Evolution of Nb-V-Mo and V Containing TRIP assisted Steels during Thermomechanical Processing. Journal of Materials Science and Technology, 33 (4). pp. 311-320. ISSN: 1005-0302

https://doi.org/10.1016/j.jmst.2016.08.019

Accepted Manuscript

Title: Microstructural Evolution of Nb-V-Mo and V Containing TRIP-Assisted Steels during Thermomechanical Processing

Author: Erfan Abbasi, William Mark Rainforth

PII: S1005-0302(16)30141-4
DOI: http://dx.doi.org/doi: 10.1016/j.jmst.2016.08.019
Reference: JMST 782

To appear in: *Journal of Materials Science & Technology*

Received date: 3-3-2016
Revised date: 18-4-2016
Accepted date: 20-4-2016

Please cite this article as: Erfan Abbasi, William Mark Rainforth, Microstructural Evolution of Nb-V-Mo and V Containing TRIP-Assisted Steels during Thermomechanical Processing, *Journal of Materials Science & Technology* (2016), http://dx.doi.org/doi: 10.1016/j.jmst.2016.08.019.

Microstructural Evolution of Nb-V-Mo and V Containing TRIP-assisted Steels during Thermomechanical Processing

Erfan Abbasi*, William Mark Rainforth

Department of Materials Science and Engineering, The University of Sheffield, Sir Robert Hadfield Building, Mappin Street, Sheffield S1 3JD, UK

[Received 3 March 2016; Received in revised form 18 April 2016; Accepted 20 April 2016]

* Corresponding author. Ph.D.; Tel.: +44 742 382 7043.

E-mail address: engabasi@gmail.com (E. Abbasi);

(W. M. Rainforth).

The microstructural evolution and precipitation behaviour of Nb-V-Mo and single V containing transformation induced plasticity assisted steels were investigated during thermomechanical processing. A plane strain compression testing machine was used to simulate the thermomechanical processing. Microstructures were characterised by optical microscopy, scanning-transmission electron microscopy and microanalysis, and X-ray diffraction analysis, and Vickers hardness was obtained from the deformed specimens. The resulting microstructure of both Nb-V-Mo and V steels at room temperature primarily consisted of an acicular/bainitic ferrite, retained austenite and martensite surrounded by allotriomorphic ferrite. The TEM analysis showed that a significant number of Nb(V,Mo)(C,N) precipitates were formed in the microstructure down to the finishing stage in Nb-V-Mo steel (i.e. 830 °C). It was also found that the V(C,N) precipitation primarily occurred in both ferrite and deformed austenite below the finishing stage. The results suggested that Nb-Mo additions considerably increased the temperature stability of microalloy precipitates and controlled the microstructural evolution of austenite. However, the microalloy precipitation did not cause a significant precipitation strengthening in both Nb-V-Mo and V steels at room temperature.

Key words: Microalloyed TRIP-assisted steel; Thermomechanical processing; Precipitation behavior; Microstructural evolution

1. Introduction

Hot rolled TRIP-assisted steel strip is frequently produced through hot rolling, followed by a rapid cooling after the final rolling pass to the bainite transformation range[1,2]. The cooling stage should be sufficiently rapid to minimise any transformation during cooling, allowing

transformation to bainite at the isothermal hold[3]. The bainite transformation is associated with carbon partitioning into austenite. This increases the stability of austenite against martensite transformation, which leads to the retention of austenite at room temperature. A combination of hard phases, such as bainite and martensite, and soft ferrite in addition to the TRIP effect of retained austenite result in a steel with high strength and high formability.

Further improvements to the mechanical properties of these steels (strength and formability) are still sought, particularly with respect to adiabatic deformation due to the high strain rate deformation commonly occurring during passenger car collisions. Attention has focussed on the effect of microalloying element additions to manipulate the microstructure and improve the mechanical properties of these steels. Microalloy carbide precipitates with a higher temperature stability (e.g., Nb(C,N) and Ti(C,N)) can be widely formed in austenite, which are especially useful in controlling the microstructural evolution during thermomechanical processing at high temperatures[4-6]. The extensive microalloy carbide precipitation, in particular vanadium carbide/carbonitride, at lower temperatures can significantly increase the strength of steels[7,8].

Investigations in alloy design of microalloyed steels have shown the influence of a combination of Mo and other microalloying elements on dynamic precipitation and precipitate coarsening[9-13]. The Mo reduces the carbon activity in austenite, increasing the solubility of microalloying elements in austenite and facilitating finer precipitation in the ferrite temperature range. Precipitation at lower temperatures leads to denser and finer precipitates, which enhances steel strength. Additionally, the Mo could decrease the interfacial energy of carbides (e.g., Nb(C,N)), which subsequently enhances the precipitation and reduces the rate of precipitate coarsening.

Although many investigations have been carried out on the single microalloy addition during thermomechanical processing, relatively few works have been reported on the precipitation behaviour of multiple microalloy additions[14-17]. It has been documented in the literature that the multi-additions of microalloying elements can change the precipitation behaviour[7]. This is of particular importance in the context of microalloyed TRIP-assisted steels because of the interaction between strong microalloy carbide/carbonitride formers and the evolution of microstructure. However, in multiple microalloyed steels, it is difficult to precisely predict the precipitation behaviour during thermomechanical processing due to the interaction between microalloying elements.

In this work a systematic study was conducted through controlled thermomechanical processing to investigate the V(C,N) precipitation behaviour in TRIP-assisted steels with an expected microstructure of an acicular/bainitic ferrite matrix. There has been no study of

microstructural evolution of Nb-V-Mo containing TRIP-assisted steels during thermomechanical processing. For the purpose of analysis, a comparison was made between Nb-V-Mo and V containing steels to better understand the effect of 0.04 wt% Nb and 0.08 wt% Mo additions on the microstructural evolution and subsequent properties of 0.16 wt% V microalloyed TRIP-assisted steels.

2. Experimental Procedure

2.1. Materials

The materials used in this investigation consisted of two as-cast microalloyed steels, prepared by laboratory melting. The chemical compositions of these steels are listed in Table 1.

The ingots were soaked at 1250 °C for 1800 s in an argon atmosphere and rough rolled from 30 to ~13 mm thick plates by 5 to 7 passes using a Hille-rolling mill with a finishing temperature of approximately ≥900 °C, followed by air cooling. Plane strain compression (PSC) testing machine equipped with a controllable heating-cooling system was used to systematically simulate thermomechanical processing. Standard PSC specimens with a size of 60 mm × 30 mm × 10 mm were machined from the rough rolled specimens. The PSC testing was carried out using the thermomechanical compression (TMC) machine at the University of Sheffield. 5-min soaking at 1250 °C was conducted before PSC testing to obtain a similar initial structure in all specimens and to dissolve the microalloy precipitates (Fig. 1(a)). Three deformation stages were applied at different temperatures with a finishing pass at 830 °C (designated "hot rolled"). In the second schedule, the specimen was held for 50 s at 900 °C to investigate the microstructural evolution and subsequent precipitation behaviour for two different microalloyed steels (designated "controlled rolled"). The effect of controlled rolling down to the end of the finishing rolling stage on the microalloy precipitation behaviour and austenite evolution was more specifically studied by water quenching the specimens immediately after the last finishing pass (designated "water quenched"). All three deformations within the PSC testing were performed at a strain rate of 10 s^{-1}. The PSC stress-strain curves were plotted after processing the recorded machine force-displacement data according to the measurement good practice guide[18].

2.2. Characterisation methods

Specimens after thermomechanical processing were cut (Fig. 1(b)), ground and polished according to standard methods (ASTM E3-11). The characterisation of microstructure, precipitation behaviour and mechanical properties at room temperature were undertaken by optical microscopy, scanning-transmission electron microscopy (SEM-TEM) and microanalysis, X-ray diffraction (XRD) and Vickers hardness testing.

To observe the prior austenite grain boundaries in water quenched specimens, the polished samples were etched with saturated aqueous picric acid at 65-75 °C for 120 s. The prior austenite grain size was measured using the linear intercept method according to ASTM E112.

Secondary electron imaging was undertaken using an FEI-Inspect F scanning electron microscope at 20 kV after etching the samples by 2% nital reagent. More details of microstructure and precipitates were studied by TEM using a series of FEI-Tecnai-20 at 200 kV and JEOL2010 field emission gun (FEG) at 200 kV. The presence of heavy elements, e.g., Nb, V and Mo in precipitates was analysed by electron dispersive spectroscopy (EDS). The electron energy loss spectroscopy (EELS) microanalysis was also used to investigate the presence of nitrogen in precipitates. The TEM analysis was conducted using thin foil and carbon extraction replica samples. TEM samples were prepared by standard methods. The chemical composition, crystal structure, size distribution and number density of microalloy precipitates were studied using carbon extraction replica samples. The low energy-loss spectrum was used to estimate TEM specimen thickness by the Kramers–Kronig Sum-Rule[19].

The average volume fraction of retained austenite was estimated by XRD using a D5000 Siemens X-ray diffractometer with CoK_α radiation. XRD data were obtained from 40° to 130° with a scanning rate of 0.1°/min and a step size of 0.02°. The characterisation of retained austenite was performed using Rietveld refinement by the Topas Academic package software V5.0. The quality and accuracy of the Rietveld refinement were checked using the numerical value of Goodness of Fit and characteristic difference pattern from the observed and calculated patterns.

Vickers hardness and micro-hardness testing were determined according to ASTM E 92-82 and ASTM E384-11 using a Universal hardness and Mitutoyo testers, respectively. The hardness testing was performed on polished specimens, while micro-hardness testing was carried out on lightly etched specimens in order to better understand the hardness of different constituents in the microstructure. The hardness and micro-hardness of specimens were measured with 20 s of holding time before unloading and two different loadings of 10 kg and 100 g, respectively. Average Vickers hardness and micro-hardness were calculated from at least ten measurements per each specimen. The size of micro-indentations was measured by both optical microscopy and 3D optical microscopy. The 3D optical microscopy was carried out using a Bruker Contour GT-K1

(with a nanometer vertical resolution) under vertical scanning interferometer (VSI) mode with a threshold of 0.1% and 30 μm back-scan.

3. Results and Discussion

3.1. Microstructure

Fig. 2(a–d) gives micrographs of the deformed regions of PSC specimens from the elongation direction (ED) after the hot rolling and controlled rolling. As can be seen from Fig. 2 the evolution of allotriomorphic ferrite in the microstructure of Steel 1 was different from Steel 2. Quantitative metallography (according to ASTM E562-11) showed that the average volume fraction of allotriomorphic ferrite was clearly higher in Steel 2 than that in Steel 1 (i.e. ~10-20 and ~17-40 vol.% in Steel 1 and Steel 2, respectively).

The fraction of allotriomorphic ferrite appeared to correlate with the extent of recrystallisation in the austenite, which was observed in Steel 2, promoting more allotriomorphic ferrite than in Steel 1, where recrystallisation was suppressed (Fig. 2). While this was mainly due to the difference in austenite grain boundary area, it could also be related to the effect of V and Nb-V-Mo additions on precipitation or solute drag that could control the kinetics of ferrite formation[20-22].

A comparison between the microstructure of deformed and undeformed regions of the PSC specimens indicates the effect of deformation on the elongation of prior austenite grains and the acceleration of the kinetics of allotriomorphic ferrite formation (Fig. 2). Optical microscopy observations of the undeformed regions of Steel 1 revealed that the allotriomorphic ferrite had hardly formed in the microstructure (Fig. 2(e)). By contrast, in an identical condition the allotriomorphic ferrite was observed in the undeformed microstructure of Steel 2 (Fig. 2(f)). This is consistent with the recent findings of Hinton et al. in 2012, who showed that Nb reduces the kinetics of ferrite formation[23]. Following the analysis of the deformed/undeformed regions of PSC specimens, it can be suggested that the effect of NbMo on retarding the allotriomorphic ferrite was partly neutralised by the mechanical deformation. In this context, the effect of V(C,N) precipitates on pinning the allotriomorphic ferrite boundaries in Steel 2 will be further elucidated in section 3.3.

Fig. 2(g) and (h) shows optical micrographs of the water quenched specimens. The micrographs indicate the prior austenite grain boundaries, suggesting the concurrent recrystallisation and elongation of austenite grains in Steel 2. Although the recrystallisation-stop

temperature was not investigated for Steel 1, the present micrographs clearly show that the deformation at 1000 and 830 °C did not cause recrystallisation, resulting in elongated prior austenite grains. This indicates that the Nb addition in Steel 1 was effective in preventing recrystallisation for the conditions used in this study.

SEM was used to further investigate the microstructure. As shown in Fig. 3, the microstructure mainly comprised acicular/bainitic ferrite and martensite. Therefore, the cooling rate of ~12 °C/s after the finishing pass was rapid enough to retain austenite down to the bainite start temperature after both hot and controlled rolling. However, some of the remaining austenite would have transformed to bainite and martensite during subsequent cooling after the isothermal hold. SEM of the microstructure of water quenched samples is shown in Fig. 3(e) and (f). In this case, the lath shaped features containing small particles in SEM micrographs were considered to be bainite. TEM and XRD analysis showed the microstructure in SEM micrographs comprised martensite, bainite and retained austenite (e.g., Figs. 4 and 5). However, the reason for bainite formation in the water quenched steels is not currently clear and needs further investigations.

3.2. Retained austenite

A considerable amount of retained austenite was formed in the microstructure after the hot rolling, controlled rolling and water quenching in both steels, as shown by XRD. Table 2 compares the average volume fraction and average carbon content of retained austenite in terms of the thermomechanical processing used. The XRD analysis generally suggested a goodness of fit of around three for all samples. The carbon content of retained austenite was determined using the following equation[24]:

$$a_\gamma = 0.35467 + 0.00467 \text{ wt\% C} \quad (1)$$

The amount of retained austenite in Steel 1 was higher than Steel 2 for all conditions. This suggests that NbMo significantly contributed to increasing the proportion of retained austenite. This is in agreement with the results of Zarei-Hanzaki et al., who also reported the effect of Nb on the austenite retention in 0.22C, 1.55Si, 1.55Mn (wt%) TRIP steel[25]. They pointed out that the solid solution hardening by Nb and work hardening of austenite at temperatures below the recrystallisation-stop temperature increases the stability of austenite against martensite transformation. In the present study, the optical micrographs of the water quenched structure showed a recrystallised structure in Steel 2. In contrast, this behaviour was absent in Steel 1. It is

therefore inferred that the strengthening of prior austenite in Steel 1 due to NbMo additions and perhaps the absence of softening mechanisms of recovery/recrystallisation might be the reasons for the stabilisation of austenite[26]. Nevertheless, it is impossible to be absolutely sure about the effect of other mechanisms such as bainite transformation on austenite retention during different cooling conditions in the studied steels (see Fig. 1 (a)). Further investigations into the bainite transformation would be required to better understand these variations.

3.3. Microalloy precipitates

In both steels, TEM-EDS analysis revealed random precipitation in the grain interiors of polygonal ferrite, but with different densities (e.g. Fig. 5). TEM observations also evidenced the presence of V(C,N) on the grain boundaries of polygonal ferrite in Steel 2 (Fig. 5(c)). These results suggested that V(C,N) precipitates in Steel 2 could retard the growth of allotriomorphic ferrite by pinning the boundaries.

The TEM-EDS analysis strongly suggested the presence of V carbide/carbonitride precipitates in the acicular/bainitic ferrite with a random distribution, though locally high density dislocations often obscure the precipitates (Fig. 5(b)). As V carbide/carbonitride precipitation hardly occurs below the bainite start temperature, it can be suggested that these precipitates formed in austenite[27, 28]. Also, the EELS analysis of precipitates in water quenched specimens showed that no significant V nitride/carbonitride was formed in the microstructure. It can be therefore inferred that V carbide/carbonitride precipitates in austenite were mainly formed at temperatures below the finishing stage (i.e. at 830°C). No systematic investigation has been reported on the possibility of V(C,N) precipitation in austenite during controlled rolling in TRIP-assisted steels at temperatures at and below the intercritical range. Recently, a few works have been reported on Nb precipitation in austenite and bainite[6,28-31]. They showed the possibility of Nb(C,N) formation in austenite at different temperatures, in particular on pre-existing dislocations (dislocation cores) and boundaries.

Locally a high dislocation density was observed in different regions of lath shaped ferrite and martensite of both steels. The high strain rate (i.e. 10 s^{-1}) and rapid cooling after finishing stage (at an average of ~12 °C/s) might limit the extent of recovery, leaving the dislocations piled up at regions close to the boundaries and microalloy precipitates. It was also likely that many of these dislocations were formed by a plastic relaxation as a result of shape strain during the bainite transformation or due to an elastic strain accommodation in the martensitic lath structure[26,32]. This indicates that the dislocations in prior austenite would be moved away from their original

positions (e.g. Fig. 5(a)). Therefore, it is impossible to make a definitive statement as to whether or not the observed precipitates were primarily formed on dislocations. However, it should be noted that the micrographs of carbon replicas are related to the precipitates, which were extracted from acicular/bainitic ferrite, allotriomorphic ferrite and martensite. This simply means that the microalloy precipitates extracted from the acicular/bainitic ferrite represented the precipitates, which had formed in austenite.

Fig. 6 gives typical carbon extraction replica micrographs showing the presence of microalloy precipitates in both steels. TEM analysis of microalloy precipitates showed that the precipitates have an FCC crystal structure in both steels (e.g., Fig. 6(g)). Fig. 6(c) and (f) shows the true shape of the ionisation edge after subtracting the background from the edge in EELS spectra. It was also found from the TEM-EDS-EELS analysis that the precipitates in Steel 1 were primarily Nb(V,Mo)(C,N) and V(C,N), and in Steel 2 they were V(C,N). Also, very few Mo carbide precipitates appeared in Steel 1, though other types of precipitates such as Mo containing V carbides were not observed in the microstructure. The Cu and Fe peaks were present in the EDS spectra. The Cu peaks are related to the TEM holder and copper grid and the Fe peaks in replica samples arose from the extraction of iron during the etching process. Although TEM micrographs showed a 2D projected image from the 3D shape of microalloy precipitates, the morphology of the precipitates in both steels did not significantly change in terms of the thermomechanical processing schedule used.

Fig. 7 shows the size distribution histograms of microalloy precipitates of Steels 1 and 2. Note that the precipitate size distribution histograms did not differentiate between precipitates of different compositions. However, the average diameter and the peak in the precipitate size distribution in Steel 1 increased after controlled rolling (i.e., from 5-10 nm to 10-15 nm). Additionally, the precipitate size distribution in the water quenched specimen showed similar behaviour to the controlled rolled specimen. This was a good evidence to confirm the consistency of results in samples subjected to a holding time of 50 s at 900 °C with an identical prior thermomechanical processing history. Also, no significant variation was observed in the average number density of precipitates in Steel 1 in terms of thermomechanical processing (Table 3). It is therefore clear that the Nb-Mo additions considerably increased the temperature stability of microalloy precipitates. Also, the kinetics of growth-coarsening of precipitates in Nb-V-Mo containing steel was primarily influenced by the growth-coarsening of existing precipitates during the holding time before the finishing stage.

As expected, very few V(C,N) precipitates (i.e. 229 precipitate μm^{-3}, with the highest frequency at 5–10 nm) were found in the water quenched specimen of Steel 2 (Table 3). Moreover,

the number density of precipitates in Steel 1 was higher than Steel 2 in water quenched samples, showing a significant precipitation in Steel 1 at higher temperatures (Fig. 7 and Table 3). The presence of NbV and NbVMo carbide/carbonitride in water quenched Steel 1 suggested that V could be partly consumed at high temperatures (i.e. ≥830 °C). These results demonstrate that the matrix of Steel 2 was supersaturated with V, available for V(C,N) precipitation mainly below the finishing stage (i.e. 830 °C). Similarly, Balliger and Honeycombe's studies on interphase precipitation showed the possibility of V(C,N) precipitation in austenite during the formation of ferrite[33]. These results are also consistent with the findings of Crooks et al., who reported on the kinetics of V and V-Nb precipitation, and austenite recrystallisation at temperatures over 800 °C[34]. They showed that the nose of the C-curve for V(C,N) precipitation in deformed austenite in a set of HSLA steels containing 0.1C (0.016-0.026)N (0.1 or 0.2)V (wt%) is lower than 800 °C. Similarly, they observed very few precipitates in specimens held for 60 s at 885 °C.

The observed difference in the precipitate number densities of hot and controlled rolled Steel 2 suggested that there was a factor reduced the extent of V(C,N) precipitation during controlled rolling (Table 3). As discussed earlier, TEM thin foil analysis evidenced that it was possible for V(C,N) to precipitate in both austenite and allotriomorphic ferrite. However, it is highly probable that the cooling rate was too rapid to allow a considerable V(C,N) precipitation.

3.4. PSC stress-strain curves at finishing pass

The PSC stress-strain curves of hot/controlled rolled specimens at 830 °C showed an increase in the peak stress of Steel 1 compared to Steel 2, though no significant difference was observed between two thermomechanical processing schedules (Fig. 8). In Steel 2, the microstructure of water quenched specimen showed a recrystallised structure with no significant microalloy precipitation at temperatures above the finishing temperature (Table 3). In contrast, the microstructure of Steel 1 contained an elongated prior austenite (i.e. pancaked grains) and a large number of microalloy precipitates (Fig. 2). It can be therefore inferred that the higher peak stress of Steel 1 corresponds to the higher work hardening, resulting from the microalloying elements and dislocations-dislocations interactions[35-38].

Additionally, the flow and peak stresses of Steels 2 for the hot rolled and controlled rolled conditions were similar at deformation pass of 830 °C. These showed that during the interpass hold time at 900 °C recrystallisation did not occur and perhaps it was stopped at temperatures over 900 °C. This is consistent with the findings of Sellars who reported a temperature around 1000 °C for the recrystallisation-stop temperature for a given C-Mn steel[20].

3.5. Vickers hardness

As shown in Fig. 9, the hardness of water quenched specimens is significantly higher compared to the other specimens. According to microscopy observations, this effect was attributed to the dominant bainite and martensite structure.

Of particular note was that the hardness of Steel 2 was not significantly lower than that of Steel 1 after the hot rolling and controlled rolling, despite the fact that the higher volume fraction of allotriomorphic ferrite was present in Steel 2 (Fig. 9). The 3D optical microscopy successfully showed the edges of micro-hardness indentations (Fig. 9(a)), though an etched surface in conventional optical microscopy often obscures the edge of indentations. Micro-hardness measurements showed a hardness of 282±33 HV0.1 for the dark regions of optical micrographs (Fig. 2). However, the large standard deviation of micro-hardness (i.e. 33 HV0.1) can be mainly related to the inhomogeneous distribution of martensite, bainite, retained austenite and precipitates in these regions. In other words, different constituents in multiphase steels have different hardness and their volume fraction and distribution can change the overall hardness[39,40]. It can be thus inferred that the most likely reasons for the high hardness of Steel 2 was attributed to the martensite/bainite volume fraction and also precipitation strengthening. V(C,N) precipitation in Steel 2 might offset the softening effect of ferrite. This is inconsistent with the earlier conclusions about the average number density of precipitates in the section 3.3. This suggests that the average number density of V(C,N) precipitates (i.e. 229 to 2400 precipitate μm^{-3}) was too low to significantly increase the hardness of steel. These results are in agreement with the findings of Hui et al., who also reported on the effect of cooling rate on the V(C,N) precipitation hardening in microalloyed medium carbon content steels[41]. They showed no considerable V(C,N) precipitation hardening in steels with acicular ferrite matrix after cooling at a rate of 10 °C/s.

4. Conclusions

(1) No significant V(C,N) precipitation was observed in the water quenched specimen of V steel (i.e., 229 precipitate μm^{-3}), whereas in Nb-V-Mo steel the majority of Nb(V,Mo)(C,N) precipitates had formed down to this stage (i.e. 830 ˚C). These results suggested that Nb-Mo additions considerably increased the precipitation temperature of microalloy precipitates in Nb-V-Mo steel.

(2) The controlled rolling led to the growth of microalloy precipitates in Nb-V-Mo steel compared with the hot rolled condition. This showed that the precipitation and growth of Nb(V,Mo)(C,N) precipitates effectively occurred at temperatures above the finishing pass, i.e. 830 °C.

(3) Microscopy observations evidenced that the microalloy precipitates in Nb-V-Mo steel considerably controlled the microstructural evolution of austenite. It was also found that both Nb-V-Mo and single V additions retarded the growth of allotriomorphic ferrite in both steels.

(4) The XRD analysis showed a significant higher retained austenite in Nb-V-Mo steel compared to V steel in all samples regardless of the effect of thermomechanical processing. This was attributed to the effect of Nb-Mo on the strengthening of austenite which stabilised the austenite against martensite transformation.

(5) The Vickers hardness of both Nb-V-Mo and V steels was similar in all thermomechanical processing conditions. The results suggested that the microalloy precipitation in both steels did not significantly increase the strength of steels at room temperature. However, in hot/controlled rolled steels, the softening effect of allotriomorphic ferrite was mainly neutralised by other strengthening contributors, i.e. martensite/bainite.

References

[1] H.J. Koh, N.J. Kim, S.H. Park, US Patent, No. 6,190,469 B1, 2001.

[2] S. Allain, A. Couturier, T. lung, Ch. Colin, US Patent, No. 2009/0107588 A1, 2009.

[3] H.K.D.H. Bhadeshia, Bainite in Steels, Transformation, Microstructure and Properties, 2nd ed., The University press, Cambridge, 2001.

[4] T. Gladman, The Physical Metallurgy of Microalloyed Steels, Maney Publishing for the Institute of Materials, Cambridge, 2002.

[5] K.I. Sugimoto, M. Murata, S.M. Song, ISIJ Int. 50 (2010) 162-168.

[6] B. Dutta, E.J. Palmiere, C.M. Sellars, Acta Mater. 49 (2001) 785-794.

[7] T.N. Baker, Mater. Sci. Technol. 25 (2009) 1083-1107.

[8] X. Deng, Z. Wang, R.D. K.Misra, J. Han, G. Wang, J. Mater. Eng. Performance. 24 (2014) 1072-1078.

[9] C.M. Enloe, K.O. Findley, C.M. Parish, M.K. Miller, B.C. De-Cooman, J.G. Speer, Scr. Mater. 68 (2013) 55-58.

[10] J.H. Jang, Y.U. Heo, C.H. Lee, H.K.D.H. Bhadeshia, D.W. Suh, Mater. Sci. Technol. 29 (2013) 309-313.

[11] J. Cao, Q. Yong, Q. Liu, X. Sun, J. Mater. Sci. 42 (2007) 10080–10084.

[12] W.B. Lee, S.G. Hong, C.G. Park, K.H. Kim, S.H. Park, Scr. Mater. 43 (2000) 319–324.

[13] L. Cheng, Q. Cai, B. Xie, Zh. Ning, X. Zhou, G. Li, Mater. Sci. Eng. A 651 (2016) 185–191.

[14] A.D. Batte, R.W.K. Honeycombe, Met. Sci. J. 7 (1973) 160-168.

[15] K. Miyata, T. Omura, T. Kushida, Y. Komizo, Metall. Mater. Trans. A 34 (2003) 1565-1573.

[16] P. Gong, E.J. Palmiere, W.M. Rainforth, Acta Mater. 97 (2015) 392–403.

[17] M. Nohrer, S. Zamberger, H. Leitner, Steel Res. Int. 84 (2013) 827-836.

[18] M.S. Loveday, G.J. Mahon, B. Roebuck, A.J. Lacey, E.J. Palmiere, C.M. Sellars, M.R. VanDerWinden, Mater. High Temp. 23 (2006) 85-118.

[19] R.F. Egerton, Electron Energy-Loss Spectroscopy in the Electron Microscope, 3rd ed., Springer, Edmonton, 1986.

[20] C.M. Sellars, in: International Conference on Hot Working and Forming Processes, Sheffield, July 3-15, 1979.

[21] G.I. Rees, J. Perdrix, T. Maurickx, H.K.D.H. Bhadeshia, Mater. Sci. Eng. A 194 (1995) 179-186.

[22] P. Yan, H.K.D.H. Bhadeshia, Mater. Sci. Technol. 31 (2015) 1066-1076.

[23] J.S. Hinton, E.J. Palmiere, W.M. Rainforth, Mater. Sci. Forum 715-716 (2012) 907-912.

[24] M.D. Meyer, D. Vanderschueren, K.D. Blauwe, B.C. De-Cooman, in: Mechanical Working and Steel Processing Conference, Baltimore, October 483-491, 1999.

[25] A. Zarei-Hanzaki, P.D. Hodgson, S. Yue, ISIJ Int. 35 (1995) 324-331.

[26] H.K.D.H. Bhadeshia, Mater. Sci. Technol. 15 (1999) 22-29.

[27] E. Abbasi, W.M. Rainforth, Mater. Sci. Eng. A 651 (2016) 822-830.

[28] I. Zuazo, S. Cobo, Mater. Sci. Forum. 706-709 (2012) 2384-2389.

[29] W.M. Rainforth, M.P. Black, R.L. Higginson, E.J. Palmiere, C.M. Sellars, I. Prabst, P. Warbichler, F. Hofer, Acta Mater. 50 (2002) 735-747.

[30] J.S. Park, Y.K. Lee, Scr. Mater. 57 (2007) 109-112.

[31] J.D.Y.J. Kim, J.G. Jung, D.H. Kim, Y.K. Lee, Acta Mater. 61 (2013) 7437–7443.

[32] L.C.D. Fielding, Mater. Sci. Technol. 29 (2013) 383-399.

[33] N.K. Balliger, R.W.K. Honeycombe, Metall. Mater. Trans. A 11 (1980) 421-429.

[34] M.J. Crooks, A.J. Garratt-Reed, J.B. Vander-Sande, W.S. Owen, Metall. Mater. Trans. A 12 (1981) 1999-2013.

[35] J.J. Jonas, Mater. Sci. Eng. A 184 (1994) 155-165.

[36] G. Fitzsimons, K. Titto, R. Fix, A.J. DeArdo, Metall. Mater. Trans. A 15 (1984) 241-243.

[37] M.G. Akben, I. Weiss, J.J. Jonas, Acta Metall. 29 (1981) 111-121.

[38] C.M. Sellars, Ironmak. Steelmak. 38 (2011) 250-257.

[39] Q. Furnemont, M. Kempf, P.J. Jacques, M. Goken, F. Delannay, Mater. Sci. Eng. A 328 (2002) 26-32.

[40] G. Cheng, K.S. Choi, X. Hu, X. Sun, Mater. Sci. Eng. A 652 (2016) 384-395.

[41] W. Hui, Y. Zhang, C. Shao, S. Chen, X. Zhao, H. Dong, J. Mater. Sci. Technol. 32 (2016) 545-551.

Figure and table captions

Fig. 1. (a) The thermomechanical processing schedules used to prepare the samples by PSC machine, (b) illustration of sectioned area from the deformed PSC sample for microstructural characterisation. ND: normal direction, ED: elongation direction, TD: traverse direction, WQ: water quenching.

Fig. 2. Optical micrographs: (a) and (b) deformation region of the hot rolled and controlled rolled Steel 1, respectively, (c) and (d) deformation region of the hot rolled and controlled rolled Steel 2, respectively, (e) and (f) undeformed region of the hot rolled and controlled rolled Steels 1 and 2, respectively, (g) and (h) water quenched specimens, showing the prior austenite grains in Steel 1 (with an average grain size of 121 μm; grain boundaries are highlighted by ImageJ software) and Steel 2 (with an average grain size of 38 μm), respectively.

Fig. 3. SEM micrographs: (a) and (b) hot rolled microstructure of Steels 1 and 2, respectively, (c) and (d) controlled rolled microstructure of Steels 1 and 2, respectively, (e) and (f) water quenched microstructure of Steels 1 and 2, respectively. α: ferrite, γ: retained austenite.

Fig. 4. Typical XRD pattern showing the peaks corresponding to the ferrite and retained austenite.

Fig. 5. Selected thin-foil transmission electron micrographs of Steels 1 and 2: (a) and (b) bright field images and typical EDS spectra, showing the presence of precipitates on the dislocations in bainitic ferrite and adjacent to retained austenite in Steel 2, (c) a dark field image and typical EDS spectrum, showing the presence of precipitates at a grain boundary in Steel 2, (d) a dark field image and typical EDS spectrum, showing the presence of precipitates in acicular/bainitic ferrite in water quenched Steel 1 (arrows indicate microalloy precipitates), (e) bright-dark field micrographs and corresponding selected area electron diffraction pattern, showing the retained austenite in Steel 2.

Fig. 6. TEM replica micrographs: (a), (b) and (c) selected TEM image and corresponding typical EDS and EELS spectra, showing microalloy precipitates in Steels 1, (d), (e) and (f) selected TEM image and corresponding typical EDS and EELS spectra, showing microalloy precipitates in Steels 2, (arrows indicate precipitates), (g) and (h) selected HRTEM images of NbVMo and V carbonitride precipitates with FCC crystal structure, respectively.

Fig. 7. Precipitate size distribution of hot rolled, controlled rolled and water quenched specimens of Steels 1 and 2, measured from carbon extraction replica samples: (a) Steel 1, (b) Steel 2.

Fig. 8. PSC stress-strain curves corresponding to the rolling pass at 830 °C in the hot rolling and controlled rolling simulations.

Fig. 9. Hardness testing results, (a) selected 3D optical micrograph, showing a topographic image of micro-hardness indentation, (b) average Vickers hardness values as a function of thermomechanical processing.

Table list:

Table 1 Chemical composition of the investigated steels (wt%)

Material	C	Mn	Si	V	Nb	Mo	N	S	P	Fe
Steel 1	0.12	1.47	1.54	0.16	0.04	0.08	0.0042	0.005	0.018	Bal.
Steel 2	0.12	1.49	1.51	0.16	-	<0.01	0.0042	0.005	0.017	Bal.

Table 2 Retained austenite parameters characterised by the XRD

Material	Thermomechanical processing	Volume fraction (vol.%)	Carbon content (wt.%)	Lattice parameter (nm)
Steel 1	Hot rolled	9.0	1.36	0.36101±0.00012
	Controlled rolled	11.3	1.33	0.36090±0.00017
	Water quenched	11.9	1.35	0.36097±0.00009
Steel 2	Hot rolled	5.2	1.32	0.36085±0.00009
	Controlled rolled	5.8	1.32	0.36083±0.00015
	Water quenched	1.9	1.35	0.36098±0.00015

Table 3 Average number density and average diameter of microalloy precipitates (measured from TEM replica micrographs)

Material	Thermomechanical processing	Precipitate number density (precipitate μm^{-3})	Average diameter of precipitates (nm)
Steel 1	Hot rolled	1538	9.5
	Controlled rolled	1306	14
	Water quenched	1400	11.5
Steel 2	Hot rolled	2400	12
	Controlled rolled	913	15
	Water quenched	229	14.5

Figure list

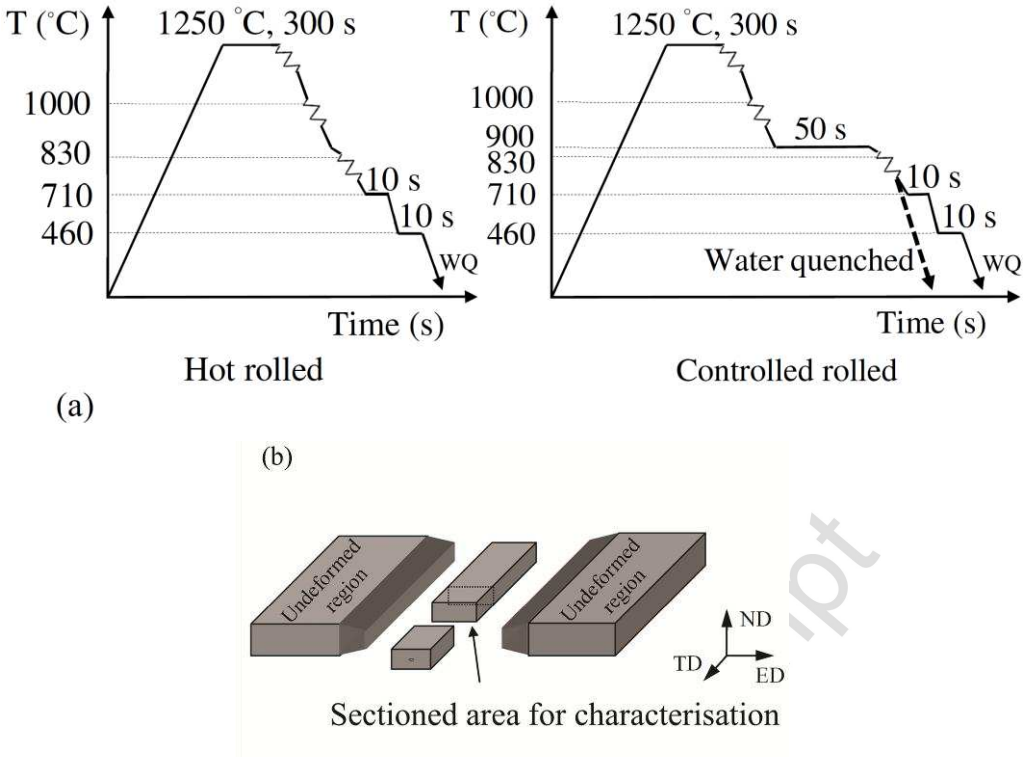

Fig. 1

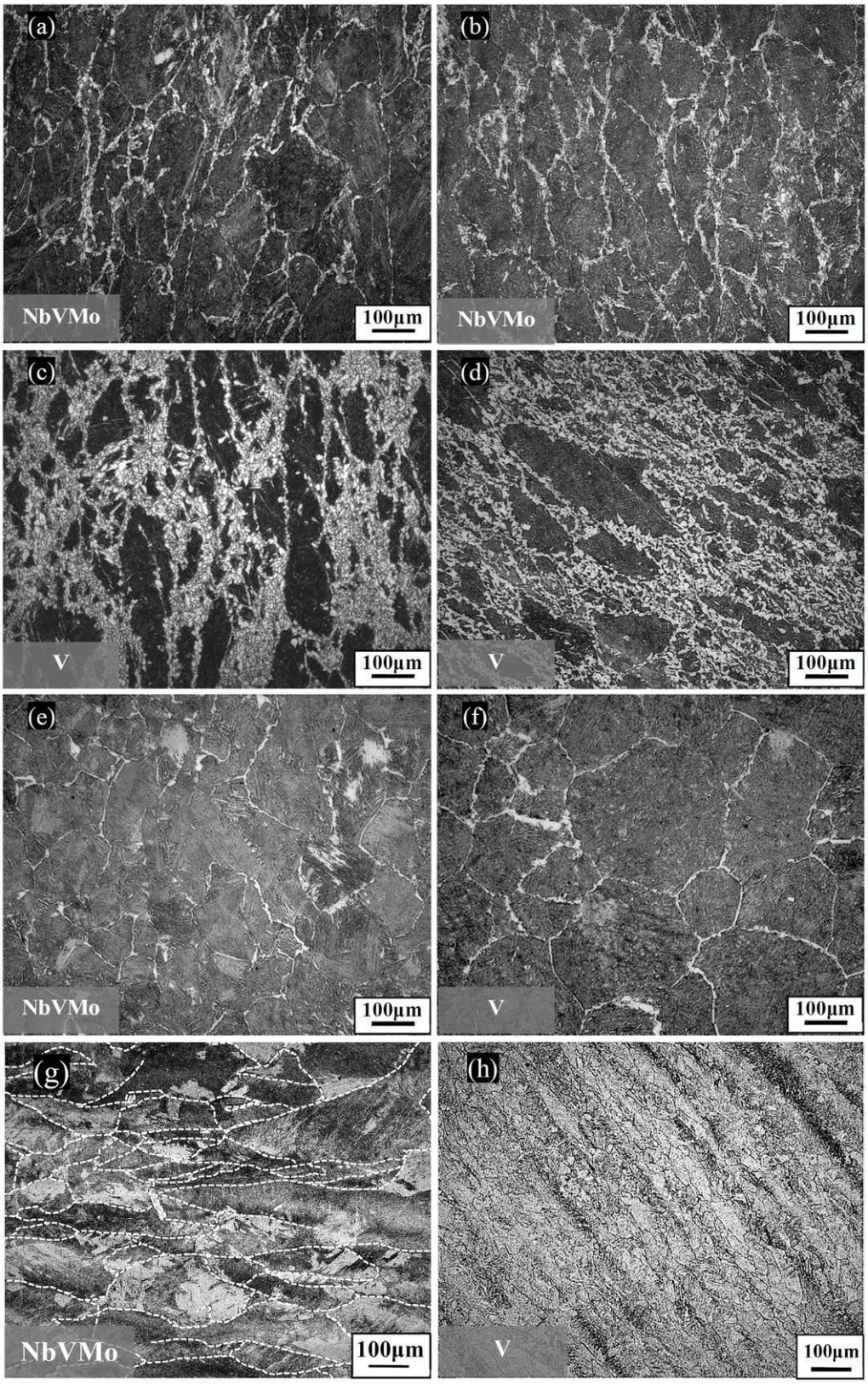

Fig. 2

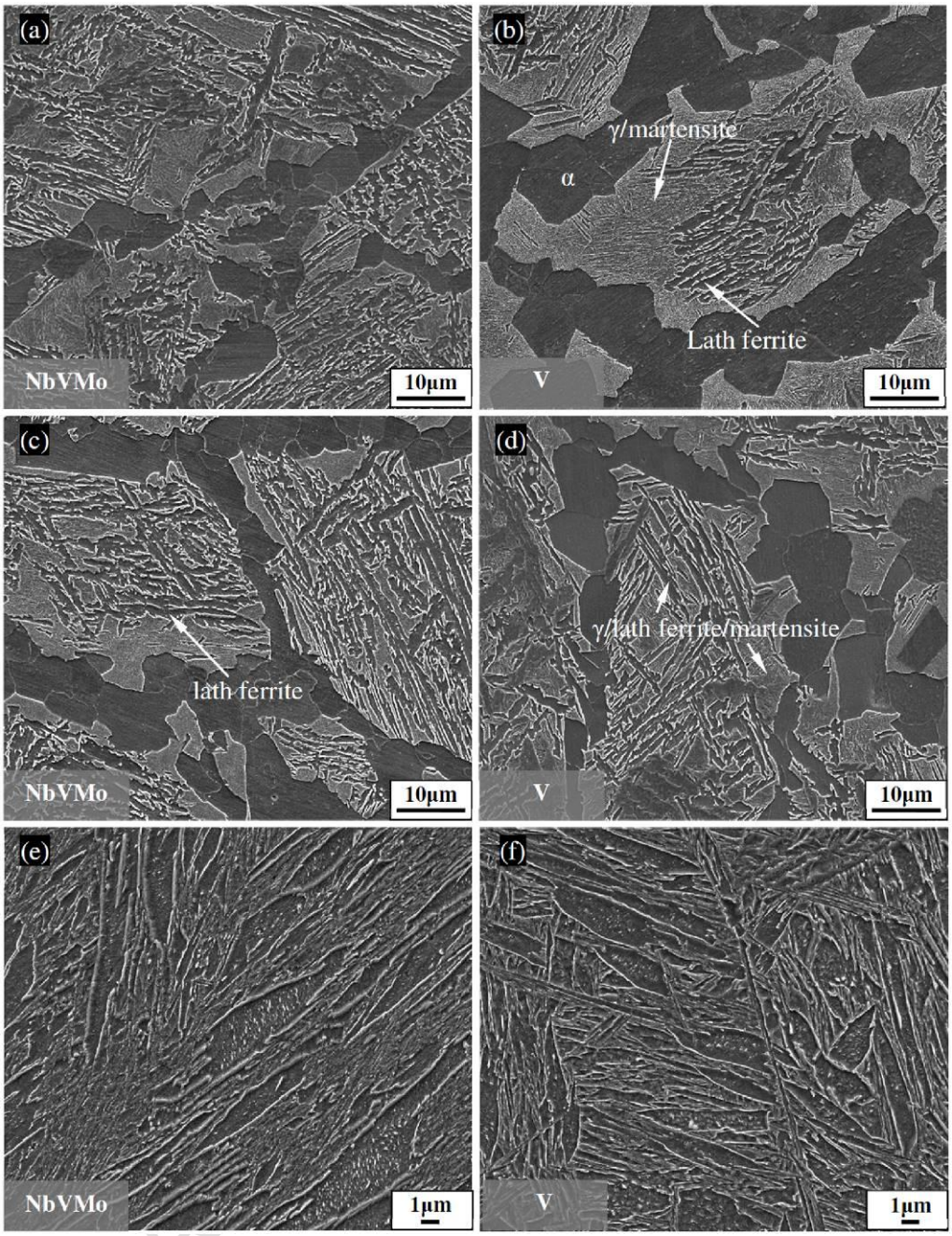

Fig. 3

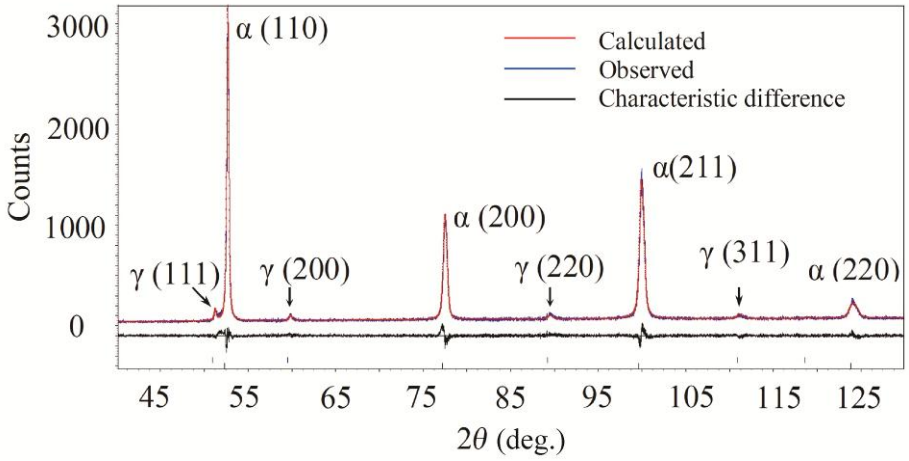

Fig. 4

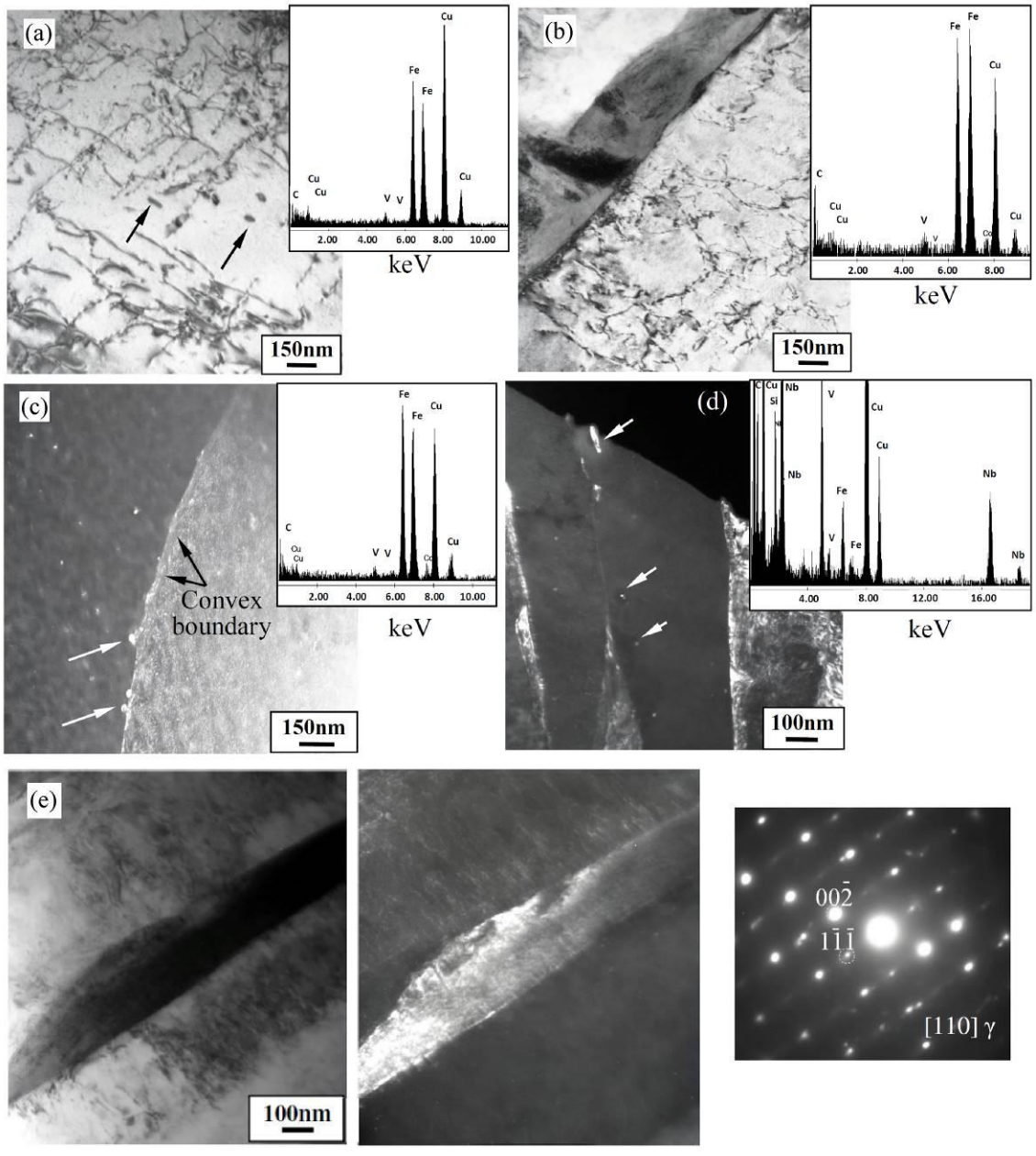

Fig. 5

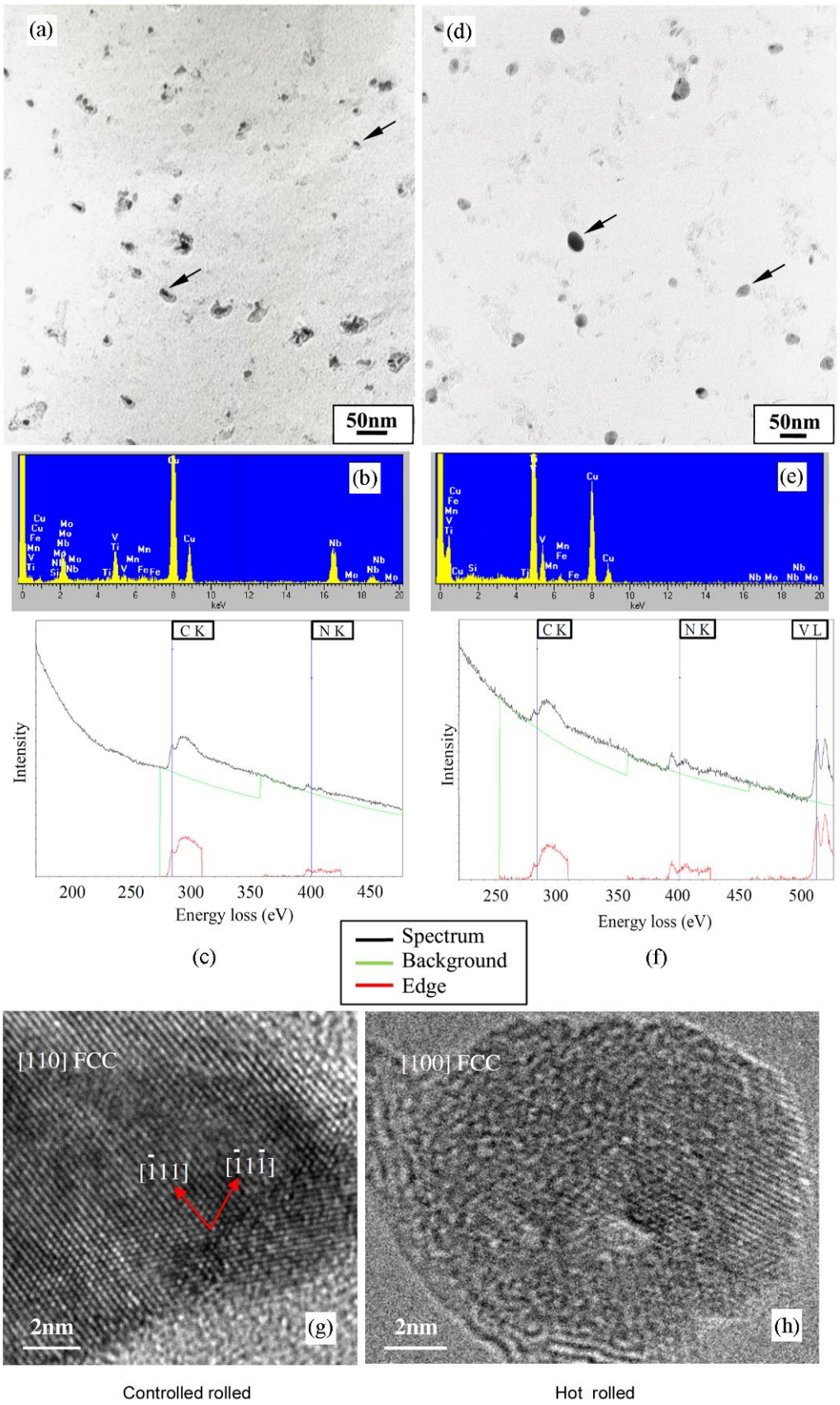

Fig. 6

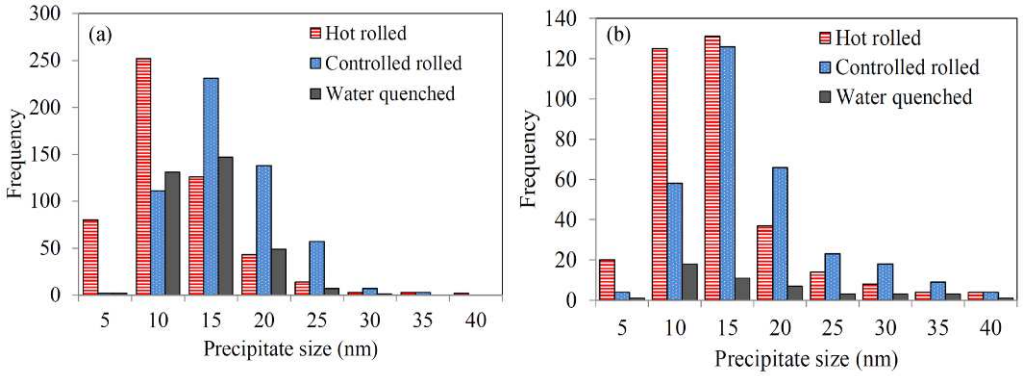

Fig. 7

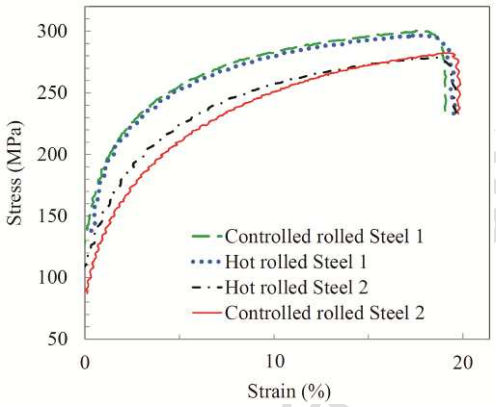

Fig. 8

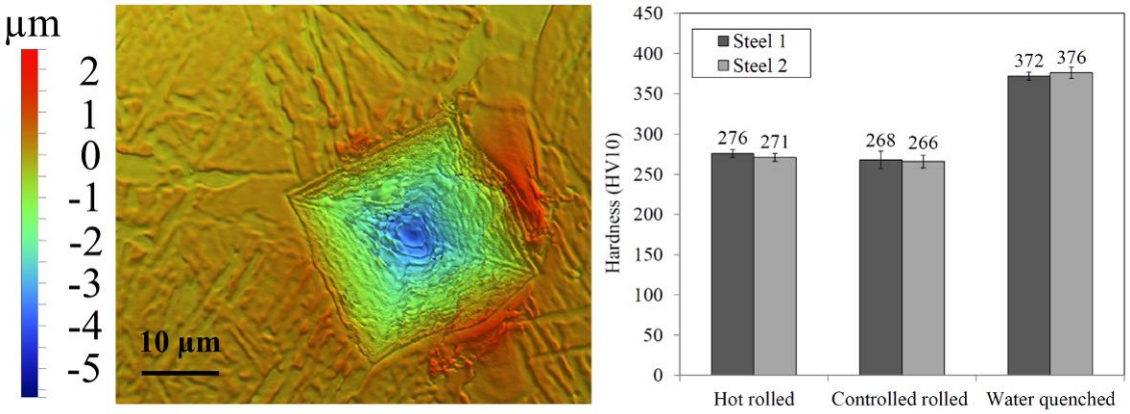

Fig. 9